Journal of Sound and Vibration (2002) **253**(3), 571–583
doi:10.1006/jsvi.2001.3982, available online at http://www.idealibrary.com on IDEAL®

EXPERIMENTAL MEASUREMENTS BY AN OPTICAL METHOD OF RESONANT FREQUENCES AND MODE SHAPES FOR SQUARE PLATES WITH ROUNDED CORNERS AND CHAMFERS

C.-H. HUANG

Department of Mechanical Engineering, Ching Yun Institute of Technology, Chung-Li, Taiwan 320, *Republic of China. E-mail: chhuang@cyit.edu.tw*

(*Received* 23 *October* 2000, *and in final form* 5 *September* 2001)

Most of the work done on vibration of plates published in the literature includes analytical and numerical studies with few experimental results available. In this paper, an optical system called the amplitude-fluctuation electronic speckle pattern interferometry for the out-of-plane displacement measurement is employed to investigate the vibration behavior of plates with rounded corners and with chamfers. The boundary conditions are traction free along the circumference of the plate. Based on the fact that clear fringe patterns will appear only at resonant frequencies, both resonant frequencies and corresponding mode shapes can be obtained experimentally using the present method. Numerical calculations by finite element method are also performed and the results are compared with the experimental measurements. Good agreements are obtained for both results. It is interesting to note that the mode number sequences for some resonant modes are changed. The transition of mode shapes from the square plate to the circular plate is also discussed.

1. INTRODUCTION

The basic principles of electronic speckle pattern interferometry (ESPI) were first proposed by Butters and Leendertz [1] to investigate the transverse vibration behavior of a disk. This technique (also called TV holography of electronic holography) is a fullfield, non-contact, and real-time method to measure the deformation for structures subjected to various kinds of loadings. As compared with the traditional holographic interferometry [2], the cumbersome and time-consuming chemical development can be omitted for ESPI and the experimental process will be speeded up. Since only $\frac{1}{30}$ s is needed to record and update a frame of interferometric pattern, ESPI is faster in operation and more insensitive to environment than holography. However, this method cannot attain the high image quality as that of the holographic interferometry due to the low resolution of the video camera system. But for practical applications, these disadvantages are outweighed by the high sampling rate of the video camera. For these reasons, ESPI has become a powerful technique used or many academic researches and engineering applications. The most widely used experimental set-up to study dynamic responses by ESPI is the time-averaged vibration ESPI method [3]. The disadvantage of this method is that the interferometric fringes represent the amplitude but not the phase of the vibration. To improve this shortcomings the phase-modulation method using the reference beam modulation technique, was developed to determine the relative phase of displacement [4, 5]. Shellabear

0022-460X/02/$35.00

and Tyrer [6] used ESPI to carry out three-dimensional vibration measurements. Three different illumination geometries were constructed, and the orthogonal components of vibration amplitude and mode shape were determined. For the purpose of reducing the noise coming from the environment the subtraction method was developed [7, 8]. The subtraction method differs from the time-averaged method in that the reference frame is recorded before vibration and is continuously subtracted from the incoming frames after vibration. In order to increase the visibility of the fringe pattern and reduce the environmental noise simultaneously, an amplitude-fluctuation ESPI (AF-ESPI) method was proposed by Wang *et al.* [9] for out-of-plane vibration measurement. In the AF-ESPI method, the reference frame is recorded in a vibrating state and subtracted from the incoming frame. Consequently, it combines the advantages of the time-averaged and subtraction methods, i.e., good visibility and noise reduction. Ma and Huang [10, 11] used the AF-ESPI method to investigate the three-dimensional vibrations of piezoelectric rectangular parallelopipeds and cylinders. Both the resonant frequencies and mode shapes were presented and discussed in details.

The investigation of plate vibrations has received considerable attention for academic research and engineering application for almost two centuries. There are hundreds of technical publications accumulated in the literature [12–14] for the free vibration characteristics of plates with various support conditions along the circumferential boundaries. Gorman [15] employed the method of superposition, which was first proposed to solve dynamic plate problems, to analyze the free vibration of a cantilever plate with various aspect ratios. Two families of mode shapes, symmetric and antisymmetric types, were described by mode contour plots and excellent convergence to exact values was shown in his work. In 1978, Gorman [16] applied the same method to investigate the vibration analysis of completely free rectangular plates, which overcomes the difficulty to satisfy the governing differential equation and boundary conditions simultaneously. Three families of modes and eigenvalues for the first six modes are illustrated with various plate aspect ratios. Irie *et al.* [17] utilized a so-called series-type method to solve the natural frequencies and mode shapes numerically for irregular-shaped plates. The variation of eigenvalues and mode shapes for these plates, which include cross-, I- and L-shaped plates, are presented according to the shape parameters. Irie *et al.* [18] also studied the free vibration of regular polygonal plates with simply supported edge by the method proposed in reference [17]. The resonant frequencies and mode shapes of polygonal plates can be obtained numerically by considering the dynamic analogy with similar membranes. It should be pointed out that the mode shapes of polygonal plates with the number of edges larger than six are similar to those of circular plates. Irie *et al.* [19] employed the Ritz method to investigate the resonant frequencies to square membranes and square plates with rounded corners for the simply supported or clamped boundary condition. The resonant frequencies of the rounded plates are between the values of circular and square plates under the same boundary conditions, except for some special cases discussed in the literature. Maruyama and Ichinomiya [20] used the time-averaged holographic interferometry to measure the resonant frequencies and corresponding mode shapes of I-shaped plates under the clamped boundary condition. The frequency parameters versus dimensionless length parameters are shown graphically and compared with the numerical results or a rectangular plate.

In this paper, the optical method based on the AF-ESPI is employed to study experimentally the free vibration of plates with rounded corners and with chamfers. The boundary conditions along the circumferential edge are traction free. Only a few papers have been published in the literature on the vibration analysis for irregular-shaped plates up to higher modes. The advantage of using the AF-ESPI method is that both resonant frequencies and the corresponding mode shapes can be obtained simultaneously from the

experimental measurement. In addition to the AF-ESPI experimental technique, numerical computations based on a finite element package are also presented and good agreements of resonant frequencies and mode shapes are found. The transition of mode shapes from a square plate to a circular plate is illustrated. On making a comparison of the vibration behavior between the plates with rounded corners and with chamfers, it is interesting to find that for some modes the shape of corners does not affect the resonant frequencies.

2. THEORY OF AF-ESPI FOR OUT-OF-PLANE VIBRATION MEASUREMENTS

The optical arrangement of ESPI for out-of-plane vibration measurement is shown schematically in Figure 1. When the specimen vibrates periodically, we record the first image as a reference. The light intensity of this reference image detected by a CCD camera can be expressed as [21]

$$I_1 = \frac{1}{\tau}\int_0^{\tau}\left\{I_A + I_B + 2\sqrt{I_A I_B}\cos\left[\phi + \frac{2\pi}{\Lambda}(1+\cos\theta)A\cos\omega t\right]\right\}\mathrm{d}t, \tag{1}$$

where I_A is the object light intensity, I_B the reference light intensity, τ the CCD refresh time, ϕ the phase difference between the object and reference light, Λ the wavelength of laser, θ the angle between object light and observation direction, A the vibration amplitude and ω the angular frequency

Let $\Gamma = 2\pi/\Lambda\,(1+\cos\theta)$ and $\tau = 2m\pi/\omega$, m is an integer, then equation (1) can be worked out as

$$I_1 = I_A + I_B + 2\sqrt{I_A I_B}(\cos\phi)\mathrm{J}_0(\Gamma A), \tag{2}$$

where J_0 is a zero order Bessel function of the first kind.

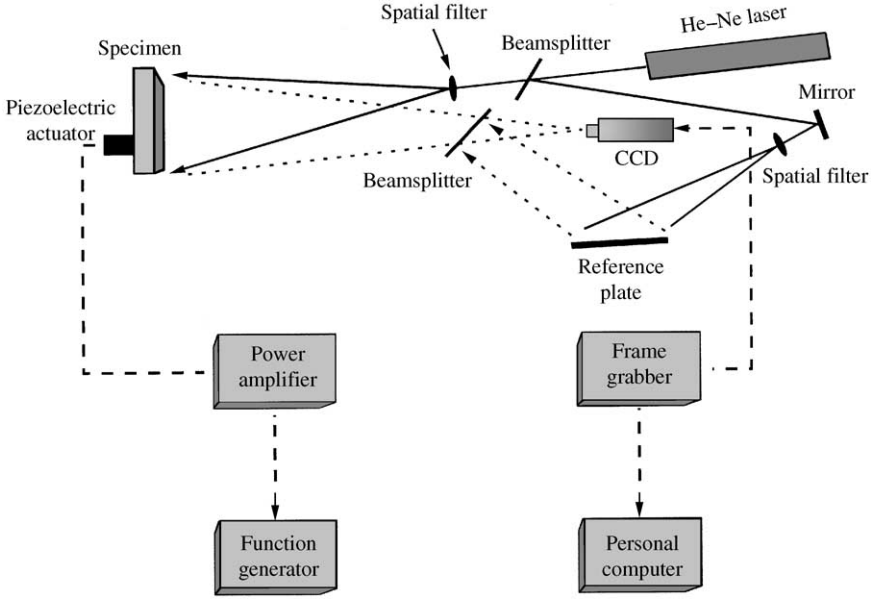

Figure 1. Schematic diagram of ESPI set-up for out-of-plane displacement measurement.

After image processing and rectifying, the intensity of the first image can be expressed as

$$I_1 = I_A + I_B + 2\sqrt{I_A I_B}|(\cos\phi)\mathrm{J}_0(\Gamma A)|. \tag{3}$$

As the vibration of the specimen goes on, we assume that the vibration amplitude has changed from A to $A + \Delta A$ because of the electronic noise or instability of the apparatus. The light intensity of the second image can be represented as

$$I_2 = \frac{1}{\tau}\int_0^{\tau} \{I_A + I_B + 2\sqrt{I_A I_B}\cos[\phi + \Gamma(A + \Delta A)\cos\omega t]\}\,\mathrm{d}t. \tag{4}$$

Expanding equation (4) using Taylor series expansion, retaining the first two terms and neglecting the higher order terms, we can rewrite equation (4) as follows:

$$I_2 = I_A + I_B + 2\sqrt{I_A I_B}(\cos\phi)[1 - \tfrac{1}{4}\Gamma^2(\Delta A)^2]\mathrm{J}_0(\Gamma A). \tag{5}$$

By image processing and rectifying, I_2 can be similarly expressed as

$$I_2 = I_A + I_B + 2\sqrt{I_A I_B}|(\cos\phi)[1 - \tfrac{1}{4}\Gamma^2(\Delta A)^2]\mathrm{J}_0(\Gamma A)|. \tag{6}$$

When these two images (the first and second images) are subtracted by the image processing system, i.e., subtract equation (3) from equation (6), and rectified, the resulting image intensity can be expressed as

$$I = I_2 - I_1 = \frac{\sqrt{I_A I_B}}{2}|(\cos\phi)\Gamma^2(\Delta A)^2\mathrm{J}_0(\Gamma A)|. \tag{7}$$

From equation (7), it is indicated that the fringe pattern for the out-of-plane vibrating motions obtained by the AF-ESPI method is controlled by a zero order Bessel function J_0. The nodal lines of vibration interferometric patterns are the brightness lines and this characteristic can be used as qualitative observation or quantitative analysis for the fringe patterns. In addition to the theory of out-of-plane measurement mentioned above, the in-plane vibration measurement by AF-ESPI method can also be derived in a similar way [10].

3. EXPERIMENTAL RESULTS AND NUMERICAL ANALYSIS

The isotropic aluminum plates (6061T6) with rounded corners are used in this study for experimental investigations and numerical calculations. The material properties of the plates are mass density $\rho = 2700\,\mathrm{kg/m^3}$, Young's modulus $E = 70\,\mathrm{GPA}$ and the Poisson ratio $v = 0{\cdot}33$. The geometric dimensions of the rounded plates are illustrated in Figure 2(a). The radius of the corner r is taken to be 5, 10, 20, and 30 mm in this analysis. For convenience, we note that R-10 represents the rounded late with radii of the corners being 10 mm. In order to increase the intensity of light reflection of specimens and the contrast of fringe patterns, the surfaces of the plates are coated with white paint that is mixed with fine seaweed powder.

A self-arranged AF-ESPI optical system as shown in Figure 1 is employed to perform the out-of-plane vibration measurement for the resonant frequency and the corresponding

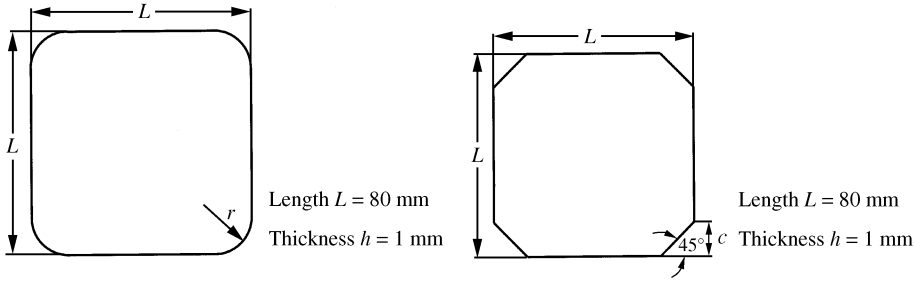

Figure 2. Geometric dimension and configuration of the (a) rounded and (b) chamfered plates.

TABLE 1

First 10 *resonant frequencies obtained from AF-ESPI and FEM for rounded plates*

	R-0		R-5		R-10		R-20		R-30		R-40	
Mode	AF-ESPI (Hz)	FEM (Hz)	AF-ESPI (Hz)	FEM (Hz)	AF-ESPI (Hz)	FEM (Hz)	AF-ESPI (Hz)	FEM (Hz)	AF-ESPI (Hz)	FEM (Hz)	AF-ESPI (Hz)	FEM (Hz)
1	494	510	507	516	521	532	579	590	670	683	792	814
2	735	745	725	746	735	746	728	750	751	768	1374	1400
3	890	945	940	957	963	987	1070	1091	1209	1233	1805	1893
4	1271	1324	1308	1340	1347	1378	1455	1500	1630	1671	3110	3171
5	2330	2357	2322	2375	2350	2418	2470	2570	2720	2815	3240	3327
6	2345	2424	2408	2456	2442	2528	2625	2707	2821	2918	4965	5112
7	2630	2634	2567	2636	2575	2641	2688	2742	2943	3003	5326	5436
8	2930	2974	2980	3048	3160	3227	3670	3786	4375	4531	5780	5922
9	3895	4021	3985	4059	4045	4130	4220	4302	4438	4579	7035	7250
10	4402	4499	4420	4501	4410	4513	4533	4652	4880	4998	7910	8154

mode shape. As shown in Figure 1, a 30-mW He–Ne laser with wavelength $\Lambda = 632{\cdot}8$ nm is used as the coherent light source. The laser beam is divided into two parts, the reference and object beam, by a beamsplitter. The object beam travels to the specimen and then reflects to the CCD camera. The reference beam is directed to the CCD camera via a mirror and the reference plate. It is important to note that the optical path and the light intensity of these two beams should remain identical in the experimental set-up. The specimen is placed on a sponge to simulate the traction-free boundary condition and is excited by a piezostack actuator. The piezoelectric actuator is usually attached by adhesive in the center of the opposite face of the specimens. However, if the nodal lines pass the center of the specimen, then the piezoelectric actuator will be moved to another location. To achieve the sinusoidal output, a function generator connected to a power amplifier is used.

Numerical results of resonant frequencies and mode shapes are carried out by using the commercially available software, ABAQUS finite element package [22]. The eight-node two-dimensional quadrilateral thick shell elements (S8R5) and reduced integration scheme are used to analyze the problem. This element approximates the Midlin-type element that accounts for rotary inertia effects and first order shear deformations through the thickness.

Table 1 shows the experimental and numerical results of resonant frequencies of the first 10 modes for rounded plates with different radii of corners. We note that R-0 represents the square plate and R-40 is the circular plate with radius 40 mm. As shown in Table 1, we can

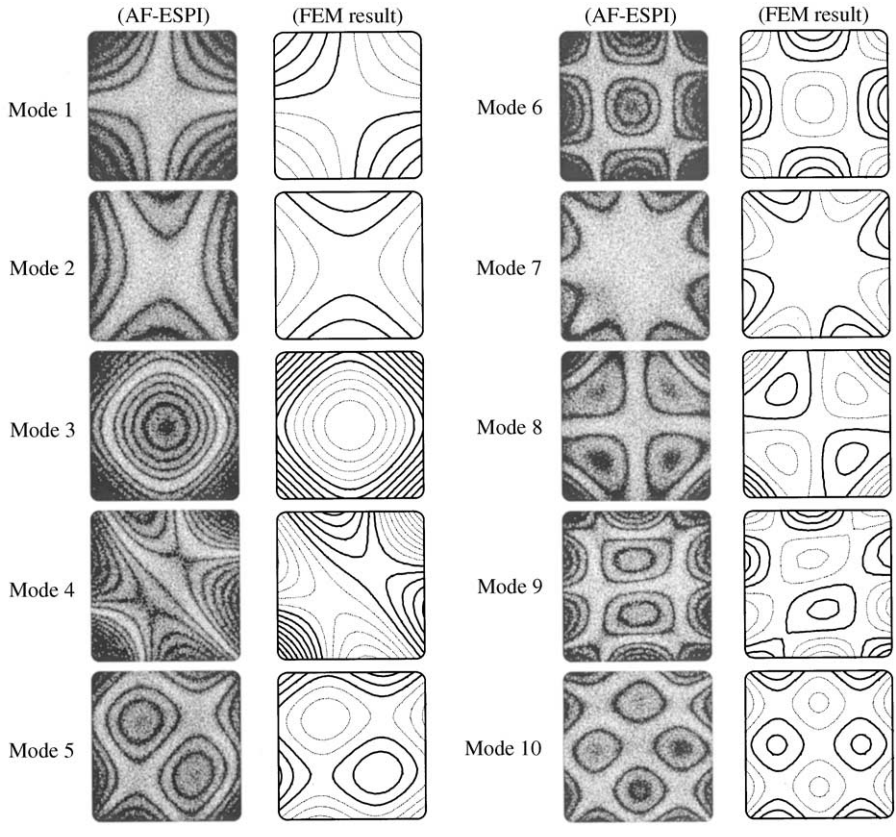

Figure 3. Mode shapes of the R-5 plate obtained by AF-ESPI and FEM.

see that these two results are quite consistent. They always have the uncertainty of the experimental determination of resonant frequencies land this may result in the opposite trend as indicated in Table 1 for R-5 and R-10 for mode 2, 7 and 10. Since the weight of the specimen increases slightly by the attached actuator, the resonant frequencies obtained from experimental measurement turn out to be lower than the numerical results. Besides, the errors are probably due to the material property measurement, the finite element approximation method and the boundary condition.

For conciseness, only experimental results of mode shapes for R-5 and R-30 plates are presented. Figures 3 and 4 show the first 10 mode shapes or both experimental measurements and numerical simulations. For the finite element calculations, the contours of constant displacement for resonant mode shapes are plotted in order to compare with the experimental observation. In Figures 3 and 4, we indicate the phase of displacement in finite element results as solid or dashed lines, where the solid lines are in the opposite direction from the dashed lines. The transition from solid lines to dashed lines corresponds to a zero displacement line, or a nodal line. The zero order fringe, which is the brightest fringe on experimental results, represents the nodal lines of the rounded plate at resonant frequencies. The rest of the fringes are contours of constant amplitudes of displacement, which can be quantitatively calculated by $J_0'(\Gamma A) = 0$ according to equation (7) for out-of-plane measurement. The mode shapes obtained by experimental results can be verified by comparing the node lines and fringe patterns with the numerical finite element calculations, and excellent agreements are found.

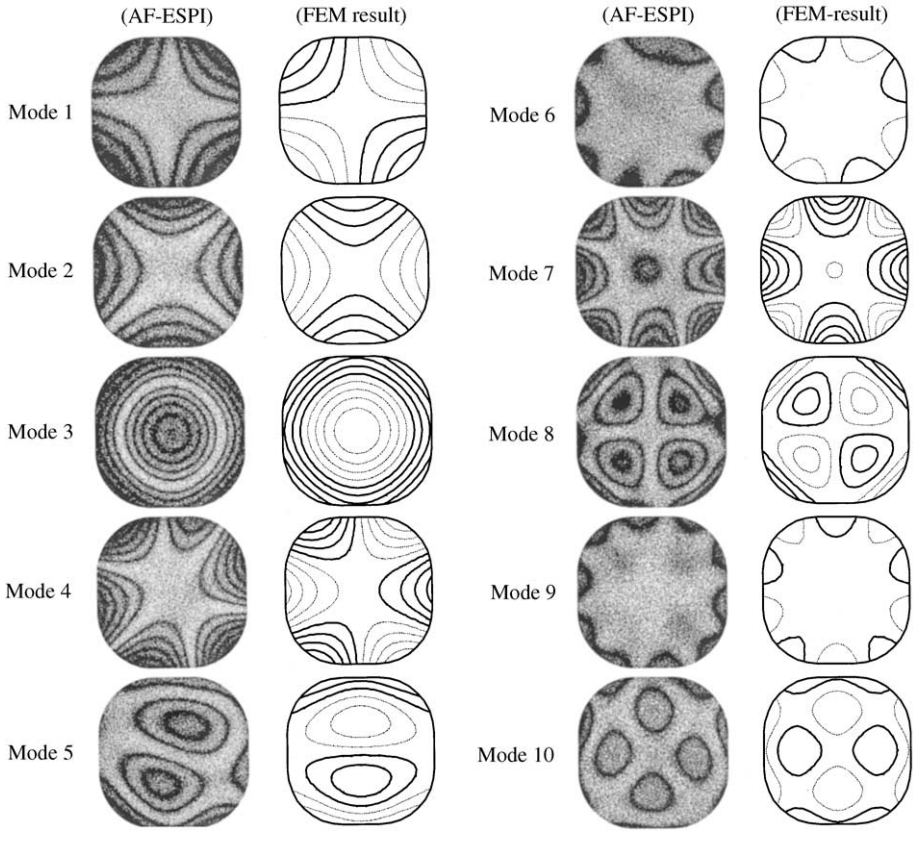

Figure 4. Mode shapes of the R-30 plate obtained by AF-ESPI and FEM.

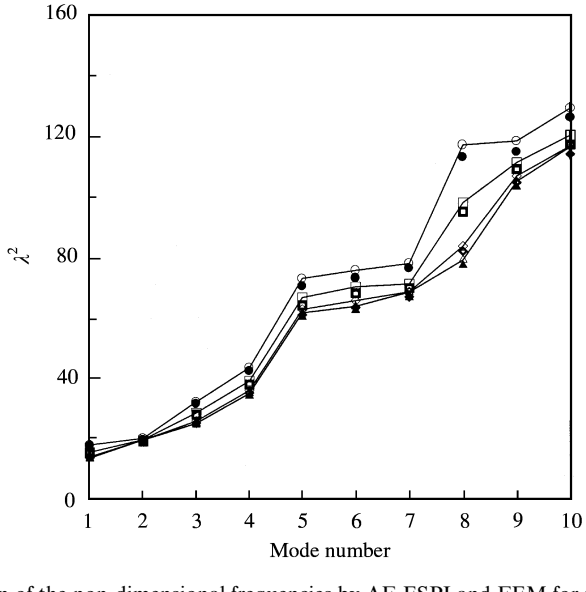

Figure 5. Comparison of the non-dimensional frequencies by AF-ESPI and FEM for the rounded plates. R-5: —△—, FEM; ▲, AF-ESPI; R-10: —◇—, FEM; ◇, AF-ESPI; R-20: —□—, FEM; □, AF-ESPI; R-30: —○—, FEM; ●, AF-ESPI.

In order to discuss the influence of the radii of rounded corners on the resonant frequency, the resonant frequency f is expressed in terms of a non-dimensional frequency parameter λ^2 given by

$$\lambda^2 = 2\pi f L^2 \sqrt{\frac{12\rho(1-\nu^2)}{Eh^2}},$$

where L is the maximum length between the opposite edges and h is the thickness of the rounded plate. Figure 5 shows the relation of non-dimensional resonant frequency and

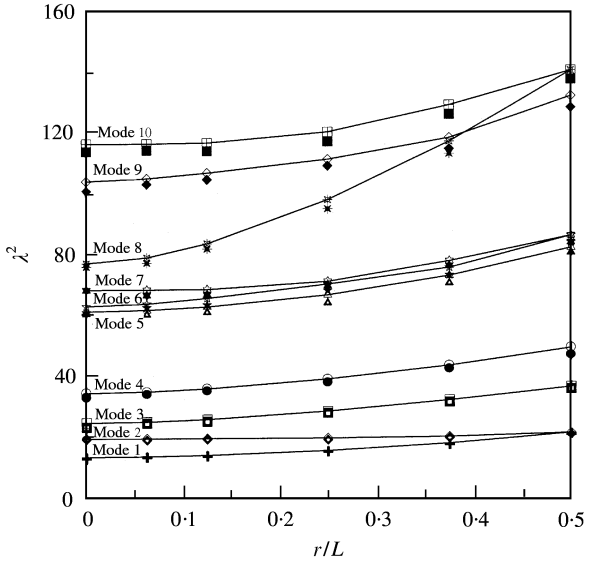

Figure 6. The results of non-dimensional frequencies for rounded plates with different radii of corners. Mode 1: —┼—, FEM; ✚, AF-ESPI; Mode 2: —◇—, FEM; ◇, AF-ESPI; Mode 3: —□—, FEM; □, AF-ESPI; Mode 4: —○—, FEM; ●, AF-ESPI; Mode 5: —△—, FEM; △, AF-ESPI; Mode 6: —☆—, FEM; ★, AF-ESPI; Mode 7: —✡—, FEM; ✸, AF-ESPI; Mode 8: —✳—, FEM; ✳, AF-ESPI; Mode 9: —◇—, FEM; ◆, AF-ESPI; Mode 10: —⊞—, FEM; ■, AF-ESPI.

TABLE 2

First 10 *resonant frequencies obtained from AF-ESPI and FEM for chamfered plates*

	Cham-0		Cham-5		Cham-10		Cham-20		Cham-30	
Mode	AF-ESPI (Hz)	FEM (Hz)	AF-ESPI (Hz)	FEM (Hz)	AF-ESPI (Hz)	FEM (Hz)	AF-ESPI (Hz)	FEM (Hz)	AF-ESPI (Hz)	FEM (Hz)
1	494	510	515	523	555	558	687	695	785	805
2	735	745	727	746	726	746	736	758	926	961
3	890	945	944	971	1010	1037	1218	1243	1432	1475
4	1271	1324	1331	1358	1405	1436	1640	1676	1960	2007
5	2330	2357	2354	2395	2414	2486	2740	2817	3305	3402
6	2345	2424	2425	2491	2575	2639	2795	2825	3380	3480
7	2630	2634	2544	2636	2600	2651	2997	3093	3605	3697
8	2930	2974	3030	3134	3415	3507	4393	4544	5096	5306
9	3895	4021	3972	4095	4125	4212	4487	4640	5375	5595
10	4402	4499	4395	4503	4396	4534	4693	4863	5748	5980

mode number for rounded plates with different radii of corners. It is interesting to note that resonant frequencies of the second mode are almost constant and resonant frequencies of the eighth mode vary drastically for the rounded plates. Figure 6 shows the dependence of frequency parameter (λ^2) on r/L for the rounded plates. Note that $r/L = 0$ represents the square plate and $r/L = 0{\cdot}5$ represents the circular plate. We find that the frequencies of the eighth mode are increasing drastically and higher than the ninth mode for $r/L > 0{\cdot}39$, which means that the orders of these two modes exchange each other. It is clearly shown in Figure 6 that some modes of the square plate will transform or reduce to the correspondent modes of the circular plate. There are three groups of mode transitions and which are expressed as follows:

Mode of the square plate		Mode of the circular plate
1, 2	$\longrightarrow$	1
6, 7	$\longrightarrow$	5
8, 10	$\longrightarrow$	7

It is indicated from these results that some modes of the square plate will combine to form the correspondent modes of the circular plate which are composed of only the nodal diameters and circles.

In this study we also investigate the vibration characteristics of the plates with chamfers for the traction-free boundary condition. The geometric dimensions of the chamfered plates

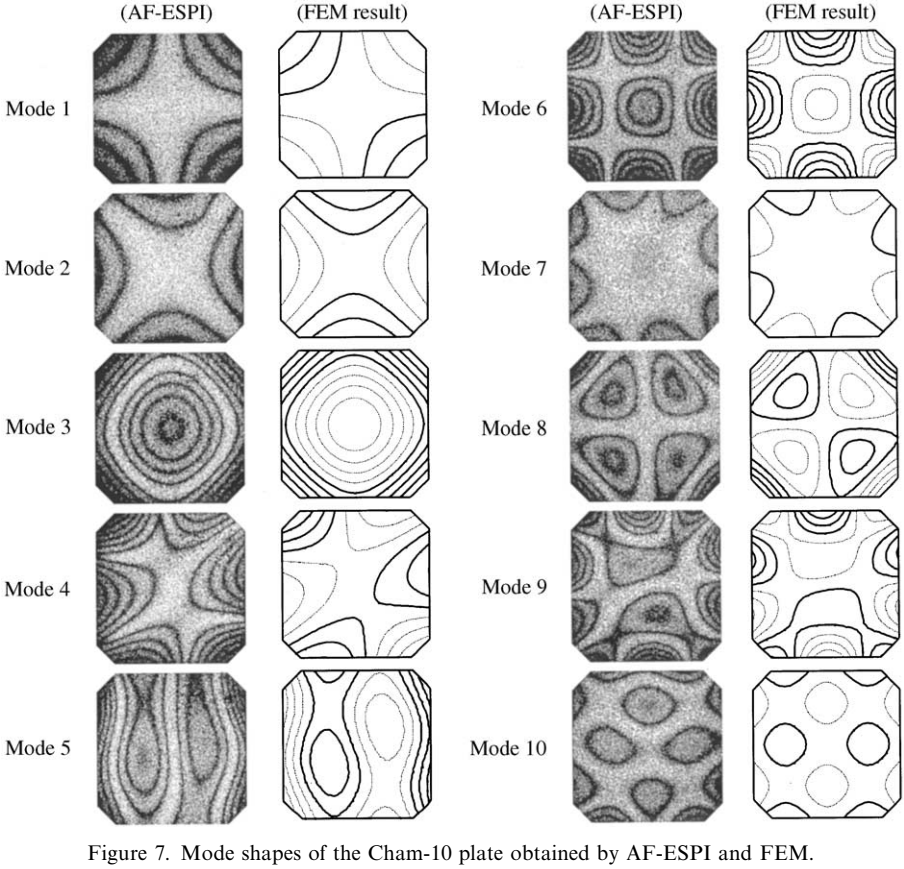

Figure 7. Mode shapes of the Cham-10 plate obtained by AF-ESPI and FEM.

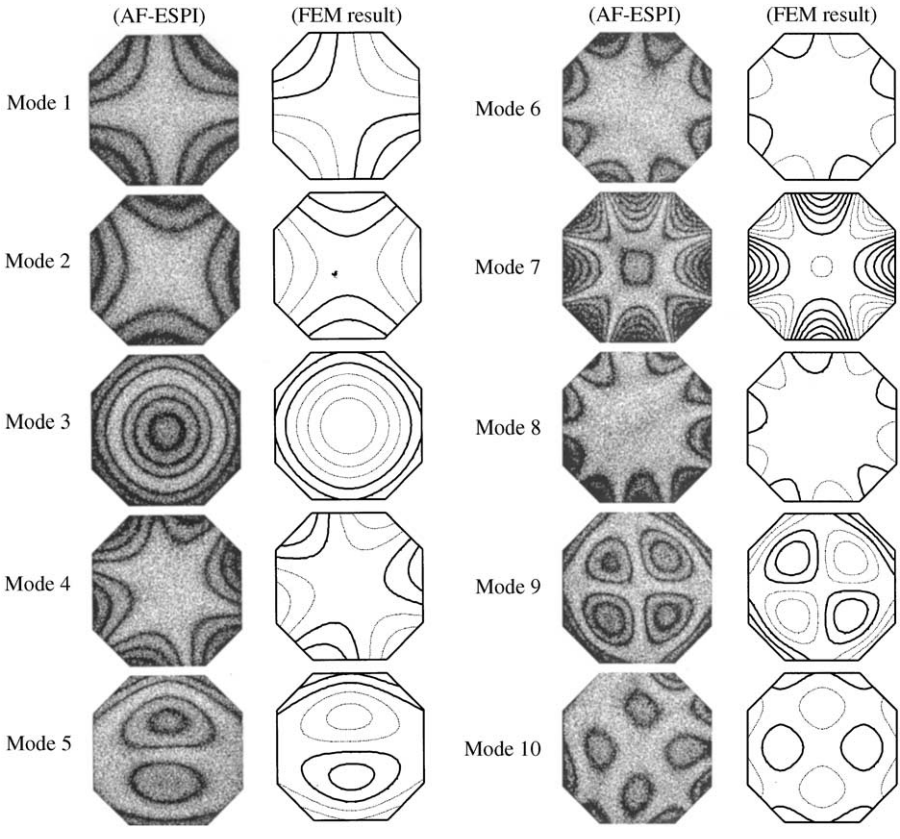

Figure 8. Mode shapes of the Cham-20 plate obtained by AF-ESPI and FEM.

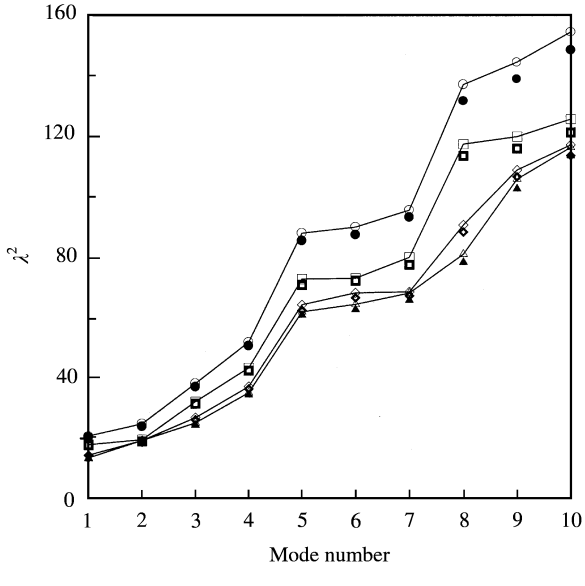

Figure 9. Comparison of the non-dimensional frequencies by AF-ESPI and FEM for the chamfered plates. Cham-5: —△—, FEM; ▲, AF-ESPI; Cham-10: —◇—, FEM; ◇, AF-ESPI; Cham-20: —□—, FEM; □, AF-ESPI; Cham-30: —○—, FEM; ●, AF-ESPI.

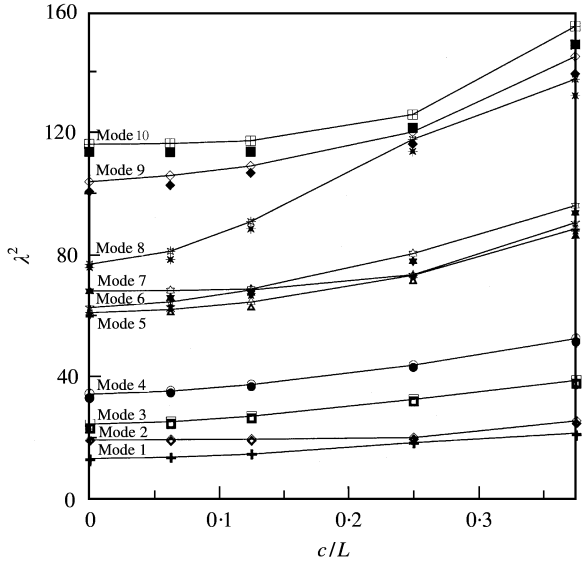

Figure 10. The results of non-dimensional frequencies for chamfered plates with different chamfer lengths. Mode 1: —┼—, FEM; ✚, AF-ESPI; Mode 2: —◇—, FEM; ◇, AF-ESPI; Mode 3: —□—, FEM; □, AF-ESPI; Mode 4: —○—, FEM; ●, AF-ESPI; Mode 5: —△—, FEM; △, AF-ESPI; Mode 6: —☆—, FEM; ★, AF-ESPI; Mode 7: —✡—, FEM; ✸, AF-ESPI; Mode 8: —✳—, FEM; ✳, AF-ESPI; Mode 9: —◇—, FEM; ◆, AF-ESPI; Mode 10: —⊞—, FEM; ■, AF-ESPI.

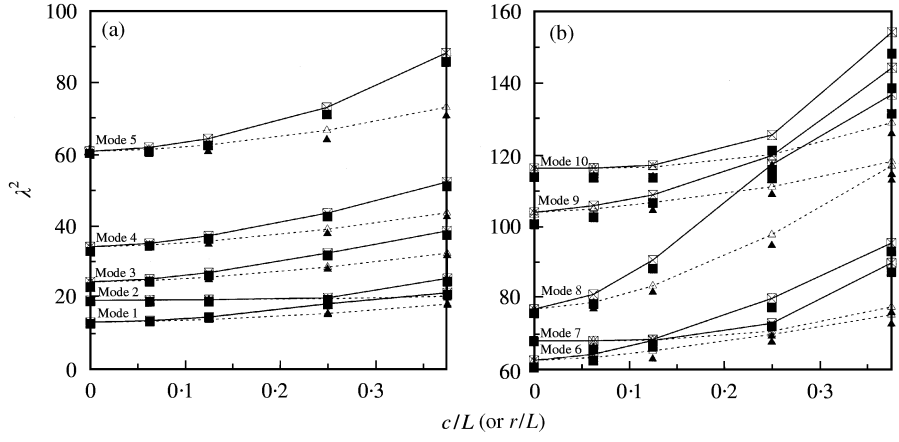

Figure 11. (a)(b) Comparison of the non-dimensional frequencies between the rounded and chamfered plates. Chamfered plates: —■—, FEM; ■, AF-ESPI; rounded plate: —△—, FEM; ▲, AF-ESPI.

are illustrated in Figure 2(b) and the lengths of chamfer c are taken to be 5, 10, 20, and 30 mm. It is indicated that the symbol Cham-10 represents the chamfered plate $c = 10$ mm. On performing the experimental procedure and numerical calculation as mentioned above, the resonant frequencies and corresponding mode shapes of chamfered plates are obtained and are compared with the numerical results. Table 2 shows the experimental and numerical results of resonant frequencies for the first 10 modes. Figures 7 and 8 are the first 10 mode shapes for the Cham-10 and Cham-20 plates. The relation of the non-dimensional frequency parameter and mode number is illustrated in Figure 9 for the chamfered plates.

Figure 10 shows the dependence of frequency parameter (λ^2) on c/L for the chamfered plates. The resonant frequencies almost increase in a similar tendency or most of the modes, except for the second and eighth modes. Besides, it is indicated that the orders of modes 6 and 7 exchange each other for $c > 10$ mm, which is similar to what occurs for modes 8 and 9 for rounded plates as mentioned above.

Finally, we discuss the difference of resonant frequencies between the rounded and chamfered plates on the condition that the radii of corners r are equal to the lengths of chamfer c. Figure 11 shows the variation of resonant frequencies between them and we can see that the resonant frequencies for chamfered plates are larger than that for rounded plates. It is also interesting to note that the resonant frequency of mode 2 is nearly a constant value for r/L (or c/L) $< 0{\cdot}25$. This means that the shapes of corners and the value for r/L (or c/L) are insensitive to the resonant frequencies of the second mode for r/L (or c/L) $< 0{\cdot}25$. A similar trend is also observed in modes 7 and 10 for r/L (or c/L) $< 0{\cdot}2$.

4. CONCLUSIONS

It has been shown that the optical ESPI method has the advantages of non-contact and fullfield measurement, submicron sensitivity, validity of both static deformation and dynamic vibration, and direct digital image output. A self-arranged amplitude-fluctuation ESPI optical set-up with good visibility and noise reduction has been established in this study to obtain the resonant frequencies and the corresponding mode shapes of irregular-shaped plates at the same time. Compared with the spectrum analysis or modal analysis method, AF-ESPI is more convenient in experimental operation. Numerical calculations of resonant frequencies and mode shapes based on a finite element package are also performed and good agreements are obtained if compared with experimental measurements. The influence of the shape of corners, which include rounded corners and chamfers, on the vibration analysis of square plates is discussed in detail. For the completely free boundary condition, the mode shapes of a square plate with round corners are shown to transform into those of a circular late, which are nodal diameters and nodal circles. The exchange of some modes in number for these two types of plates is observed. They are the eighth and ninth mode for the rounded plate and the sixth and seventh mode for the chamfered plate. From the variation of non-dimensional frequency parameter (λ^2) versus corner shape parameter (r/L or c/L), we find that the resonant frequency and mode shape of the second mode will not be affected by the shape of corners for r/L (or c/L) $< 0{\cdot}25$.

ACKNOWLEDGMENTS

The author gratefully acknowledges the financial support of this research by the National Science Council (Republic of China) under Grant NSC89-2212-E-231-004.

REFERENCES

1. J. N. BUTTERS and J. A. LEENDERTZ 1971 *Optics and Laser Technology* **3**, 26–30. Speckle pattern and holographic techniques in engineering metrology.
2. P. K. RASTOGI 1994 *Holographic Interferometry*. Berlin: Springer-Verlag.
3. R. JONES and C. WYKES 1989 *Holographic and Speckle Interferometry*. Cambridge: Cambridge University Press.
4. O. J. LØKBERG and K. HOGMOEN 1976 *Journal of Physics E: Scientific Instruments* **9**, 847–851. Use of modulated reference wave in electronic speckle pattern interferometry.

5. A. P. M. HURDEN 1982 *NDT International* **15**, 143–148. An instrument for vibration mode analysis using electronic speckle pattern interferometry.
6. M. C. SHELLABEAR and J. R. TYRER 1991 *Optics and Lasers in Engineering* **15**, 43–56. Application of ESPI to three-dimensional vibration measurements.
7. K. CREATH and G. Å. SLETTEMOEN 1985 *Journal of the Optical Society of America* **A 2**, 1629–1636. Vibration-observation technique for digital speckle-pattern interferometry.
8. B. POUET, T. CHATTERS and S. KRISHNASWAMY 1993 *Journal of Nondestructive Evaluation* **12**, 133–138. Synchronized reference updating technique for electronic speckle interferometry.
9. W. C. WANG, C. H. HWANG and S. Y. LIN 1996 *Applied Optics* **35**, 4502–4509. Vibration measurement by the time-averaged electronic speckle pattern interferometry.
10. C. C. MA and C. H. HUANG 2001 *IEEE Transactions on Ultrasonics, Ferroelectrics, and Frequency Control* **48**, 142–153. The investigation of three-dimensional vibration for piezoelectric rectangular parallelepipeds by using the AF-ESPI method.
11. C. H. HUANG and C. C. MA 1998 *American Institute of Aeronautics and Astronautics Journal* **36**, 2262–2268. Vibration characteristics for piezoelectric cylinders using amplitude-fluctuation electronic speckle pattern interferometry.
12. A. W. LEISSA 1977 *The Shock and Vibration Digest* **9**, 13–24. Recent research in plate vibration: classical theory.
13. A. W. LEISSA 1981 *The Shock and Vibration Digest* **13**, 11–22. Plate vibration research, 1976–1980: classical theory.
14. A. W. LEISSA 1987 *The Shock and Vibration Digest* **19**, 11–18. Recent studies in plate vibration: 1981–85. Part 1, classical theory.
15. D. J. GORMAN 1976 *Journal of Sound and Vibration* **49**, 453–467. Free vibration analysis of cantilever plates by the method of superposition.
16. D. J. GORMAN 1978 *Journal of Sound and Vibration* **57**, 437–447. Free vibration analysis of the completely free rectangular plate by the method of superposition.
17. T. IRIE, G. YAMADA and Y. NARITA 1978 *Journal of Sound and Vibration* **61**, 571–583. Free vibration of cross-shaped, I-shaped and L-shaped plates clamped at all edges.
18. T. IRIE, G. YAMADA and K. UMESATO 1981 *Journal of the Acoustical Society of America* **69**, 1330–1336. Free vibration of regular polygonal plates with simply supported edges.
19. T. IRIE, G. YAMADA and M. SONODA 1983 *Journal of Sound and Vibration* **86**, 442–448. Natural frequencies of square membrane and square plate with rounded corners.
20. K. MARUYAMA and O. ICHINOMIYA 1979 *Experimental Mechanics* **19**, 271–275. Experimental determination of transverse vibration modes of thin I-shaped plates.
21. R. K. ERF 1978 *Speckle Metrology*. New York: Academic Press.
22. HIBBITT, KARLSSON and SORENSEN 1995 *ABAQUS User's Manual*, *Version* 5.5. Rhode Island: Hibbitt, Karlsson and Sorensen Pawtucker.